Chapter 10
Carbonaceous Nanostructures-Based Photocatalysts for Sustainable H_2 Production

E. Nandhakumar, E. Vivek, E. Vaishnavi, M. Prem Kumar, Perumal Devaraji, P. Selvakumar, and N. Senthilkumar

1 Introduction

The consumption of fossil fuels (coal, natural gas and oil) has increased as the anomalous growth of industries, power plants and automobiles, resulting in a scarcity of fossil energy resources and triggers a serious problem such as energy crisis and global warming. As a result of this, environmental pollution and energy depletion have drawn attention to the urgent need for alternative forms of clean energy production. So, the researchers are paying considerably attention to utilize hydrogen as renewable energy source and making possibilities via photocatalytic hydrogen generation [1, 2].

E. Nandhakumar · M. Prem Kumar
School of Mechanical Engineering, Vellore Institute of Technology, Vellore 632014, India

E. Vivek
Department of Physics, University College of Engineering, BIT Campus, Anna University, Tiruchirappalli 620024, India

E. Vaishnavi
Department of Chemistry, Sri GVG Visalakshi College for Women, Udumalapet 641014, India

P. Devaraji
Henan Engineering Research Center of Resource and Energy Recovery From Waste, Henan University, Kaifen 475007, PR China

P. Selvakumar
Department of Engineering and Sciences, Western Norway University of Applied Sciences, Bergen, Norway

N. Senthilkumar (✉)
Department of Electronics and Communications Engineering, M. Kumarasamy College of Engineering, Karur 639113, India
e-mail: senthilkumarn.ece@mkce.ac.in

A. N. Grace et al. (eds.), *Handbook of Porous Carbon Materials*,
Materials Horizons: From Nature to Nanomaterials,
https://doi.org/10.1007/978-981-19-7188-4_10

Hydrogen (H_2) is a clean, eco-friendly and non-hazardous resource because while it combusts only water is produced during the combustion process [3, 4]. The generation of H_2 using a semiconductor photocatalytic technique is a promising solution for generating energy by converting solar energy to fuel [4, 5]. At first, the photocatalysis method of hydrogen production was reported by Fujishima and Honda in 1972 using Titanium dioxide (TiO_2) [6]. TiO_2 is among the most stable semiconducting material for photocatalytic hydrogen production because of its good stability and nontoxicity [7]. It has the bandgap (Eg) of 3.2 eV which offers to absorb the solar spectrum in the range of ultraviolet region [3]. In addition, the photocatalytic efficiency of TiO_2 is quietly low as of the rapid recombination occurred in the photogenerated hole pair, which hinders the practical application. Therefore, it is important to limit the charge carrier's recombination rate occurs in semiconductor photocatalyst [8]. However, the researchers are trying to improve the properties of photocatalyst through various combinations of catalyst.

On the other hand, various carbon-based nanomaterials are attracted for its high stability, wide photo-absorbance property and high conductivity. Moreover, the discoveries of carbon nanotubes (CNTs), graphene, carbon nanofibres (CNF) and other carbon materials emerge as a building block in the arena of nanotechnology [9]. Carbon can exist in the various forms like CNT, CNFs [10], horns [11], flasks [12], carbon spheres [13, 14] and calabashes [15]. Carbon-based material has a tenable combination of sp, sp^2, sp^3 hybridization [14]. Carbonaceous materials have been classified with their dimension which includes carbon dots, fullerenes, graphene, and graphite material as zero-dimensional (0D), one-dimensional (1D), two-dimensional (2D) and three-dimensional (3D) structures, respectively (Fig. 1). Along with that graphene is a marvel material with 2D structure of regular lattice arrangement with hexagonal pattern in sp^2 hybridized form of carbon atoms [16, 17]. Therefore, the carbon-based nanomaterials have great attention in the field of semiconductor-based photocatalytic method of hydrogen production.

In this chapter, we discussed the recent advancements in carbon-based nanomaterials for photocatalytic H_2 generation. We specifically discussed the different carbon materials based on their dimensions as well as the role of interface engineering between carbonaceous structures and other semiconductor nanomaterials.

2 Fundamentals of Hydrogen Evolution

2.1 Basic Principle

Three basic steps are involved in the photocatalytic process, namely (1) absorption of light and generation of photoexcited electron and holes in the valance band (VB) and conduction band (CB), respectively, and (2) separation and migration of photoexcited electron and holes to the surface of the photocatalytic materials; these two steps are deciding the efficiency of the process because the recombination of photoexcited

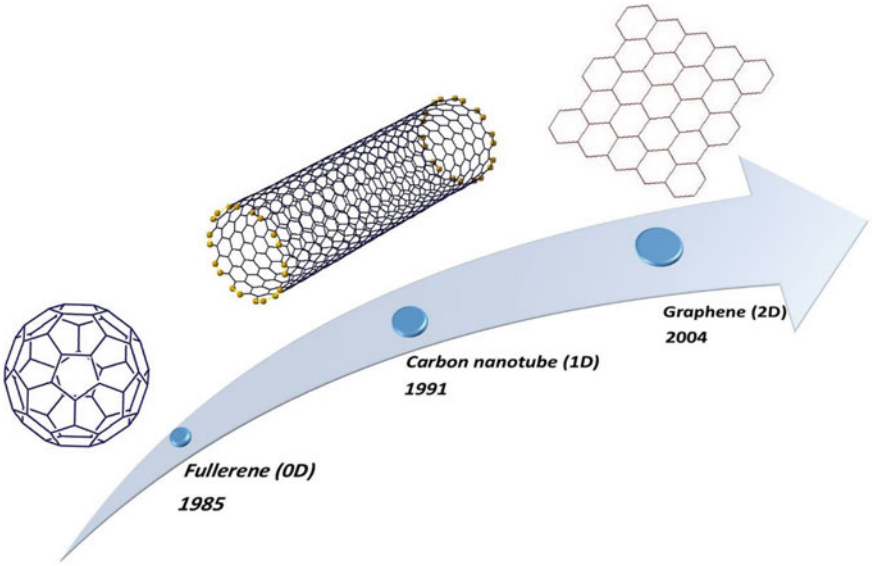

Fig. 1 Different types of carbonaceous nanostructures "Reprinted with permission from Jun et al. [18]. Copy right 2018 Elsevier"

charge carries could occur in the femtosecond in the bulk. Many semiconductor photocatalyst have been developed to enhance the charge separation efficiency which could enhance the photocatalytic activity.

For instance, noble metals such as Au, Ag and Pt [19], CdS/CdSe/Pt heterostructure, [20], Zn–Ag–In–S/Co_3O_4 [21], Cu/TiO_2 [22], (Au/AgAu)@CdS [23] are greatly mitigates the recombination rate of photoexcited charge carriers. The Schottky junction between the metal and semiconductor interface increases charge transfer and reduces recombination [19]. In addition to that, introduction of carbon-based materials such as fullerene [24] g-C_3N_4 [25] and RGO [26] to semiconductor materials predominantly increases the charge mobility and greatly reduces their recombination. The effective utilization of electron–hole pair creates for surface redox reaction. For effective reduction of proton, the conduction band potential of photocatalyst should be negative and very close to the reduction potential of proton versus normal hydrogen electrode (NHE). On the other hand, in case of oxidation of water the valance band potential of semiconductor material should be greater than the 1.23 eV versus normal hydrogen electrode. The basic process involved in photocatalyst is illustrated in Fig. 2.

The apparent quantum yield (AQY) of photocatalytic H_2 evolution is calculated based on the below formula:

$$\text{AQY}\ (\%) = \frac{\text{Number of reacted electrons}}{\text{Number of incident photons}} \times 100\% \tag{1}$$

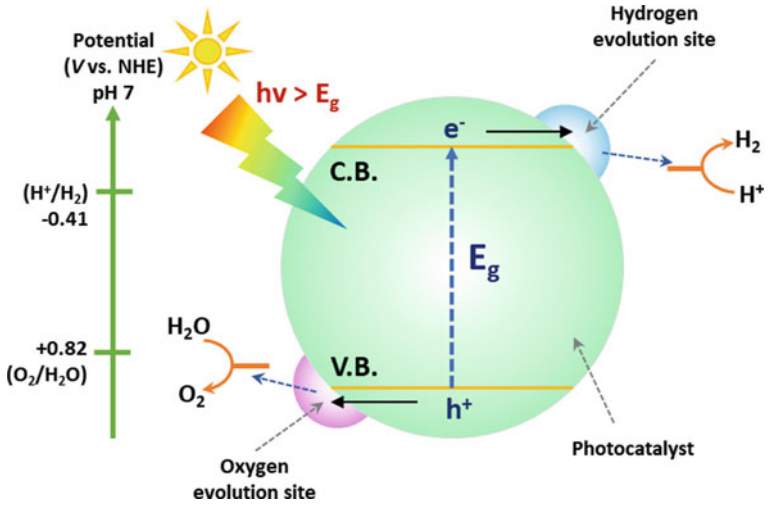

Fig. 2 Graphic representation of photocatalytic water split reaction

$$\text{AQY}\ (\%) = \frac{\text{Number of evolved } H_2 \text{ molecules} \times 2}{\text{Number of incident photons}} \times 100\% \qquad (2)$$

2.2 *Use of Sacrificial Agents*

Efficiency of photocatalysis reaction was greatly decreased by recombinations of charge carriers. Sacrificial agents such as CH_3OH, triethylenetetramine, aqueous solution of sodium sulphide and sodium sulphate could use to hinder the recombination of electron and hole. Sacrificial agents can be utilized to scavenge indeed an electron or hole for the evolution of hydrogen or oxygen. Sacrificial agents that scavenge hole, like methanol, esoteric the hole and oxidize it to CO_2. Because of this approach, electrons excited to CB have a longer lifetime and are effectively implemented for reduction. In this context, the electron scavenging reagent like silver nitrate plays a vital role which is exactly opposite to the previously mentioned hole scavenger, as the oxidation takes place of holes. Because hole scavengers have a lower oxidation potential compared to water molecules, the thermodynamical and kinetic limitations are massively diminished. It is to be understood that water splitting is an arduous process involving a change in free energy ($\Delta G = 237$ kJ/mol). Because of the large reductions in ΔG, it eliminates the four-electron process of molecular oxygen production. The nature of the sacrificial agents, as well as their oxidation/reduction potential, influences the decrease in ΔG. With environmental concerns in mind, it is also implied that methanol be replaced by eco-friendly alcohols such as glycerol and carbohydrates. The use of glycerol is highly beneficial due

to its superior hydrogen content per molecule; however, carbon to hydrogen ratio is lower than that of methanol. Nevertheless, H_2 generation via water splitting reaction through a sacrificial agent, including such glycerol or methanol, could be regarded as a simple objective as it less challenging compared to overall water splitting reaction (OWSR) without the use of a sacrificial agent [27]. Considering the OWSR's rate of advancement over the past three decades, we believe it has the potential to be a big energy-conservation solution.

2.3 Band Alignment

Another interesting technique for promoting separation of photogenerated electron–hole pairs is heterojunctions fabrication. Heterojunctions are formed by joining two photocatalysts (PC-1 and PC-2) together via mechanical or electrostatic forces, as well as chemical bonds. The interface plays a major role to ensure fast transfer of charge carriers. The semiconductor heterojunctions are classified into three types: (i) Type-I (ii) Type-II and Z-scheme heterojunctions are shown in Fig. 3. In Type-I heterojunction (Fig. 3b), the two photocatalyst are activated by incident light and then the electrons from PC-2 with higher conduction band (CB) transfers to PC-1 with lower CB position beneath the force of electrostatic field. Meanwhile, photogenerated holes are transferred from lower VB to higher VB positions. As a result, the photogenerated and holes are gathered on PC-1. In Type-II heterojunction (Fig. 3c), the transfer of electron is similar to Type-1 from PC-2 to PC-1 [28]. Moreover, the holes transfer is reverse to Type-1 from PC-1 to PC-2. For this event, the reduction reaction is occurred for PC-1 when photogenerated electrons are collected on PC-1 and the holes on PC-2 for oxidation reaction. The development of a heterojunction could result in enhance of charge separation by guiding the flow of electrons and holes at the interface. And also, the charge recombination is suppressed, thus can substantially improves photocatalytic activity [29, 30].

2.4 Surface Functionalization

Carbon nanomaterials have a propensity to agglomerate due to their high surface energy and high Van der Waals force between them. Weak dispersibility in solvents is a cause of these aggregation phenomena, which limits their application. So, carbon materials must be functionalized to modify their physiochemical properties to overcome this constraint [31]. The surface functionalization is a process of modifying the chemistry of the material surface to achieve a desire property. Depending on the types of interactions between active molecules and carbon atoms, functionalization techniques are broadly classified into physical functionalization and chemical functionalization (Fig. 4) [32]. The physical functionalization (non-covalent) techniques include high impact mixing, rubbing, high shear mixing, ultrasonication, etc. These

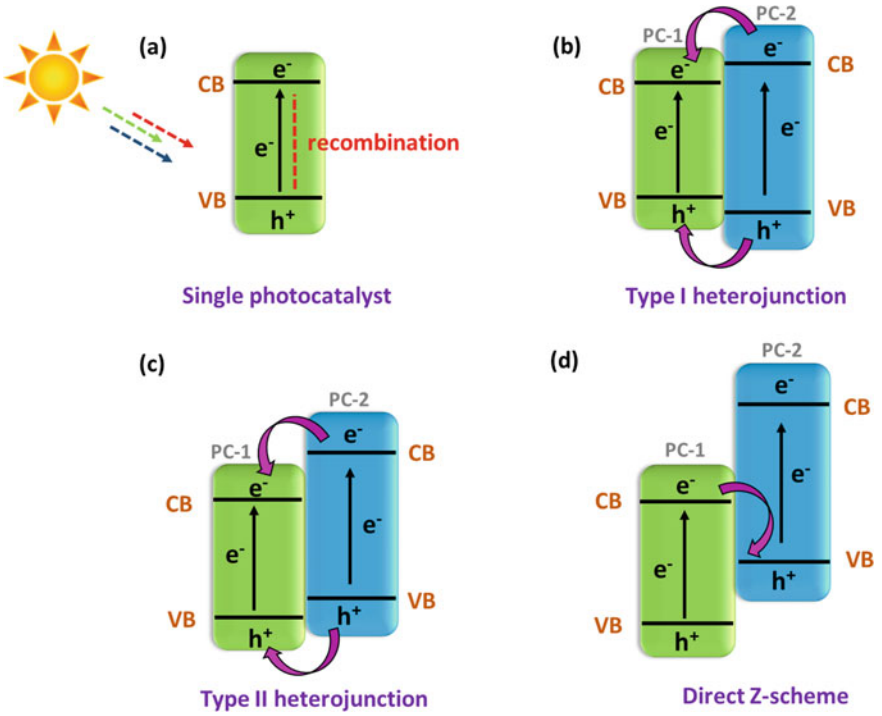

Fig. 3 Schematic diagram of semiconductor material heterojunction formation for photocatalytic hydrogen production

procedures can keep them from aggregating, but they may break apart throughout the process and lowering the aspect ratio. As a result, it is a time-consuming and ineffective approach. Chemical functionalization (covalent) is a method of attaching functional groups using covalent bonds by means of chemical treatment. This method can improve their dispersion stability and wetting or adhesion property so covalent factualization is the most preferred technique for changing the surface energy of the carbon materials without distressing its electrical, optical or mechanical properties. In this scenario, functionalizing the carbon nanomaterials using different chemical treatments is considered to be an effective strategy for improving the efficiency in the field of hydrogen generation via solar-mediated water splitting [33].

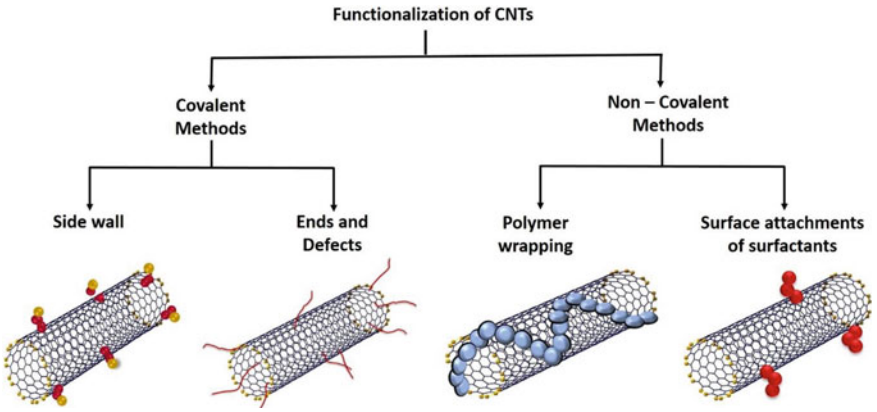

Fig. 4 Functionalization methods of carbon nanotubes "Reprinted with permission from Jun et al. [18]. Copyright 2018 Elsevier"

3 Carbon Material Nanostructure

3.1 0D Carbonaceous Materials

For the past two decades, chalcogenides quantum dots were appreciated for its opto-electrical properties and application in various fields ranging from biology to technology. However, the prominent toxicity is associated with such limits their industrial applications. Highest market cost of such toxic dots leads the new entrant carbon-based dots to be a promising alternative. The King of the element, namely carbon and their derivatives, can satisfy the profound quality in emerging economies [34, 35] The history of carbon materials revealing the chemistry of the quantum effects in 0D carbon material can solve the puzzle of their excellent properties (Fig. 5a) [36]. As a consequence of the quantum effect of matter at smaller atomic levels, discrete bandgap systems and edge effects are created with remarkable properties [37, 38].

3.1.1 Carbon Dots

Since, after the discovery by Xu et al. carbon dot research fired up its performance in photocatalysis and sensor applications [39, 40]. These sp^2 hybridized carbon materials are known for superior stability, low toxicity, and tunable optical, conducting properties, etc., [41]. Functionalizations of C-dots make them as good photon absorber and excellent electron acceptor and donor [42–44].

A blend of mixed crystal TiO_2 with carbon dots (CQD_S) was synthesized, characterized and revealed outstanding performance for H_2 production by Tang et al. [45, 46]. The yield of H_2 was 280 μ mol h^{-1}, which was higher than that using pure TiO_2 alone. CQD_S act as an electron storage medium which may enhance charge transfer

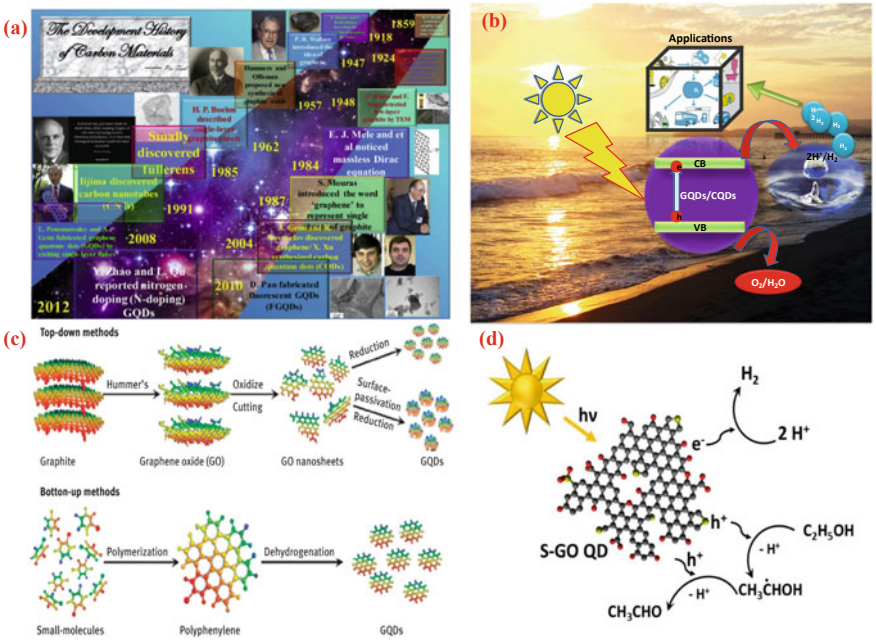

Fig. 5 **a** Evolution in carbon materials from the year 1859 to 2012 was "Reprinted with permission from Tian et al. [47]. Copyright 2018 Elsevier," **b** pictorial illustration of photocatalytic mechanism for water splitting by GQD_S and CQD_S, **c** GQD_S different synthesis approaches reproduced with permission from "Reprinted with permission from Shen et al. [48]. Copyright 2012 Royal Society of Chemistry", **d** S-doped GQDs hydrogen splitting mechanism in 80% of ethanol/aqueous medium at pH 8 reproduced with permission from reference "Reprinted with permission from Gliniak et al. [49]. Copyright 2017 Wiley"

and inhibit e^--h^+ pair recombination. The incorporation CQD_S into TiO_2 shifted the absorption and emission to visible region showing that electrons can be transferred from CQD_S to TiO_2. The inhibition of e^--h^+ recombination was proved by weaker PL spectra of CQD_S –TiO_2 system. The hydrogen treatment of CQD_S-TiO_2 exhibited a better H_2 generation activity than pure TiO_2 due to improved optical activity of CQD_S-TiO_2.

The CQDs-TiO_2 samples showed prompt photocurrent response, while hydrogen-treated CQDs-TiO_2 indicated and enhanced photocurrent response. Such an observation clearly brings out the influence of CQDs in TiO_2 on H_2 yield improvement. Siu and co-workers investigated on photocatalytic hydrogen production of CQDs/TiO_2 nanosheets with major (001) plane. Furthermore, many previous reports on carbon quantum dots composites showed superior hydrogen gas (116.1 mol g^{-1} h^{-1}) production [50, 51]. C-dots can also show high performance as co-catalyst in water splitting reaction. Wang et al. [44] reported that CQDs/g-C_3N_4 composite are well suited for enhanced hydrogen production of 2.34 mmol g^{-1} h^{-1} but g-C_3N_4 alone showed only 0.51 mmol g^{-1} h^{-1}. The catalytic efficiency is four times that of pure material. The

interaction of CDs and g/C_3N_4 hybrid improves charge transport capabilities as well as inhibits electron–hole recombination at the interface [52, 53].

Nitrogen-doped CQDs nanocomposite serves as an excellent material for photocatalytic H_2 production. In addition to the early research, the superior photocatalytic activity was illuminated under visible and NIR irradiation using N-CDs/CdS nanocomposites, where lattice acid as a sacrificial reagent (consume the photogenerated holes by providing electron). The low visible light photocatalytic H_2 evolution rate (14.8 mmol h^{-1} g^{-1}) was achieved due to their rapid electrons (CB) and holes (VB) recombination for pure CdS. Shi et al. proved that the incorporation of N-CDs could successfully separate the charge carriers of cadmium sulphide, consequently enhancing the photocatalytic performance of N-CDs/CdS. The highest photocatalytic activity was found when 5 wt% N-CDs were loaded, with an optimum H_2 evolution rate of 58.9 mmol h^{-1} g^{-1}, which is approximately 5 times greater than cadmium sulphide alone. The H_2 production rate decreased after the addition of N-CDs, which could be attributable to an excess of N-CDs covering the surface of CdS, resulting in lesser active sites for H_2 production [54]. Additionally, these heterostructure carbon dots composite materials have high durability for hydrogen production.

3.1.2 Graphene Dots (GQDs)

Graphene dots with its incredibly smaller size, less than 30 nm, behave dually as graphene and quantum dots. GQDs derived from a 2D graphene exist mostly in elliptical or circular shapes, and even some GQDs are triangular and hexagonal [55, 56]. These ultra-small GQDs with its interesting quantum confinement and edge effect properties usually emit green or blue fluorescence (quantum yields of GQDs are mostly at a range between 2 and 22.9%). These dots have superior biocompatibility, low toxicity, good chemical stability and enhanced luminescence compared to that of inorganic semiconductor dots. GQDs possess bandgaps between 2.2 and 3.1 eV [57, 58]. Figure 5c shows the traditional Nano synthesis approach for GQDs. Eco-friendly, cheapest earth-abundant carbon materials were predominantly utilized for synthesizing GQDs [59]. Since 2008, after the discovery of GQDs, many researchers have consistently made progress in systematic tailoring and functionalization. After purification and chromatographic separation, these materials can be characterized by using material science techniques. Furthermore, the resulting GQDs func*t*ion as a promising catalyst for hydrogen production and opens new prospects for carbon-based materials research Fig. 5b [60]. Figure 5d illustrates the implication of graphene dots as a photocatalytic material to split water for large-scale hydrogen generation in the near future. For example, graphene oxide (GO) has better lifetime for 200 days with photocatalytically water efficient of 575 μmol h^{-1} g^{-1} [61–63]. The contibution of graphene is more to improve the Water Splitting under light driven conditions [64]. N-doped graphene dots can be efficiently synthesized from carbon nano-onions using laser ablation method. Calabro et al. proved that the heteroatom-doped graphene resulted in an efficient catalytic property [65]. Theoretical work also suggested that tailoring the bond environment of carbon atoms in graphene by

heteroatom (boron, nitrogen and sulphur) can enrich the mobility of hole and electron, respectively, henceforth enhancing the water splitting reaction [66, 67]. Table 1 illustrates hydrogen production efficiency of graphene materials. Yeh et al. employed nitrogen-graphene oxide quantum dots for water splitting application under visible light [68–70]. The rate of hydrogen generation efficiency of sulphur-doped graphene in the presence of different sacrificial electron donors was investigated by Tung et al. The results revealed that the highest performance up to 80% was detected in ethanol/aqueous medium at pH 8. Subsequently, a plausible mechanism for the improved water splitting (30,519 $\mu mol\ h^{-1}\ g^{-1}$) and prolonged lifetime of the catalyst was justified by conducting the experiments in the presence of H_2O_2 [68, 71, 72]. In order to achieve enhanced photocatalytic performance, it is necessary to combine the graphene dots with TiO_2. Figure 6a, b illustrates the reaction mechanism of the dual role of graphene dots as a sensitizer (for efficient light absorption) or as a co-catalyst (for enhanced charge separation) on biphasic TiO_2. Compared to single-phase TiO_2, the anatase/rutile nature of P-25 TiO_2 resulted in efficient charge transfer which in turn, promotes hydrogen production rate up to 29,548 $\mu mol\ g^{-1}\ h^{-1}$. This heterojunction provides systematic separation of electron–hole pairs, in addition dots amplify the photocatalytic behaviour of TiO_2 [62, 64]. Similar to this work, many researchers investigated the graphene dots modified TiO_2 nanotubes, titania nanosheet [57, 73, 74] for enhancing the photocatalytic efficiency under UV light irradiation. Many worthwhile efforts have been made on the functioning of nitrogen-doped GQDs with TiO_2 by Yeh et al. Also, Sudhagar et al. reported the sensitizing effect of GQDs on TiO_2 nanowire and various TiO_2 nanostructure [75].

To conclude, GQDs has played an eminent role in enriching the photocatalytic H_2 evolution. Graphene dots' co-catalyst can also function as an efficient photoharvester and facilitates the improving electron transfer property. As an alternative material for TiO_2, composites of ZnO nanowire and graphene dots were replaced by many scientists and the water splitting was illustrated under solar irradiation [76]. In this system, graphene dot function as aid in harnessing the visible light as well as enhance the separation of charge carriers of metal oxide by trapping the electrons and thereby delaying the recombination of charge carrier present in TiO_2 which results in better photocatalytic performance. Fabrication of graphene dots onto the surface of metal sulphide nanoparticles was clearly explored by Tian et al. and Lei et al. [62, 76, 77]. Also, Dinda et al. reported on covalent linking of rhodamine dye with graphene dots to produce hydrogen efficiently under visible light without any co-catalyst [78]. Henceforth, the graphene dots can play a dual role as co catalyst as well as photosensitizer in H_2 evolution. Still the reason regarding the exact role of the graphene quantum dots system in hydrogen production mechanism is unclear. With current efforts to better study the behaviour of GQDs and develop new nanomaterial functionalities, it is expected that novel applications will prosper in the near future.

Table 1 Carbonaceous material-based nanocomposites for photocatalytic hydrogen production

Photocatalysts	Synthesis method	Sacrificial agents	Light source	H_2 production	References
S-graphene oxide QDs	Hydrothermal	EtOH	500 W Xe lamp	30,519 μmol g^{-1} h^{-1}	[49]
GQDs/TiO_2	Hydrothermal	Na_2SO_4	500 W Hg lamp	79.3 μmol g^{-1} h^{-1}	[79]
Lu modified ZnO/CNTs	Sol–gel	Glycerol	300 W Xe lamp (300–1100 nm)	380 μmol h^{-1} g^{-1}	[80]
CdS/Cu_7S_4/g-C_3N_4	Ultrasonication	Na_2S + Na_2SO_4	300 W Xe lamp (λ > 420 nm)	3570 μmol g^{-1} h^{-1}	[81]
Nickel-S:g-C_3N_4	Photodeposition	Triethanolamine	150 W Xe lamp	3628 μmol g^{-1} h^{-1}	[82]
g-C_3N_4/Bi_4NbO_8CI	Ball milling	Na_2SO_4	300 W Xe lamp (λ > 420 nm)	287.7 μmol g^{-1} h^{-1}	[83]
RGO/$ZnIn_2S_4$	Alcohothermal method	Na_2S, Na_2SO_4	350 W Xe lamp (420 nm)	1597 μmol g^{-1} h^{-1}	[84]
MOS_2 QDs/UiO-66-NH_2/graphene	Ultrasonication method	Triethanolamine	300 W Xe lamp (λ > 420 nm)	186.37 μmol h^{-1} g^{-1}	[85]
Boron/oxygen co-doped g-C_3N_4 nanomesh	Freeze drying method	Triethanolamine	300 W Xe lamp (λ > 420 nm)	9751 μmol h^{-1} g^{-1}	[28]

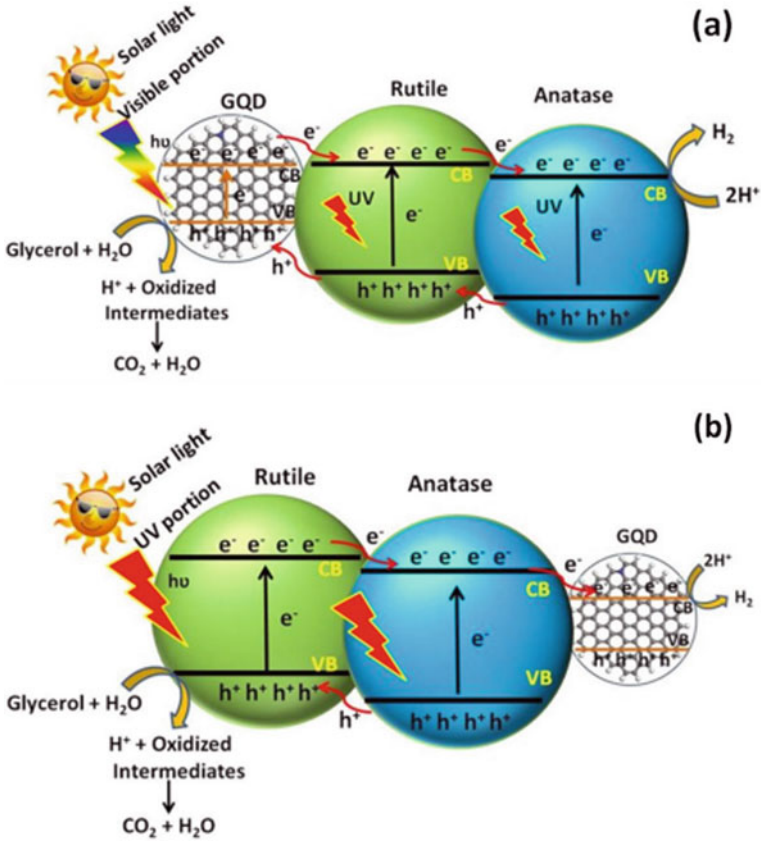

Fig. 6 **a** and **b** the enhanced hydrogen generation by decoration of graphene QDs onto the bi-phase TiO_2 nanostructures "Reprinted with permission from Raghavan et al. [64]. Copyright 2020 American Chemical Society"

Carbon Nanotubes (CNTs)

The carbon nanotubes (CNTs) were discovered in 1991 by Sumio Iijima; it offers large surface area, excellent thermal conductivity, high electron emission, high thermal and chemical stability [86–89]. In the recent past decade, CNTs employed in photocatalytic applications have both metallic and semiconducting capabilities due to the chiral indices of the CNTs [90, 91]. CNTs have the potential to solve the challenges that semiconductors have in photocatalysis.

CNTs are a one-dimensional structure of carbon allotropes; it is like tubular containing graphite. Also, CNTs are hollow cylinder, while rolling it formed single or multilayered graphene. The carbon nanotubes were classified into two types, (i) single-walled carbon nanotubes (SWCNTs) and (ii) multiwall carbon nanotubes (MWCNTs). The difference between SWCNTs and MWCNTs is listed in Table 2. A single-walled carbon nanotubes (SWCNTs) can be thought of as a single molecule

Table 2 Comparative of SWCNTs and MWCNTs properties

SWCNTs	MWCNTs
Graphene arranged in single layer	Graphene arranged in multi-layer
For synthesis catalyst is required	It is possible to produce without catalyst
Difficult to do bulky synthesis required suitable growth control and environment condition	Easy to synthesis in bulk
During functionalization defect should be more	When using the arc-discharged technique, the chances of defect is reduced
SWCNTs can be easily twisted	MWCNTs cannot be easily twisted
It is easy for evaluation and characterization	It has very complex structure

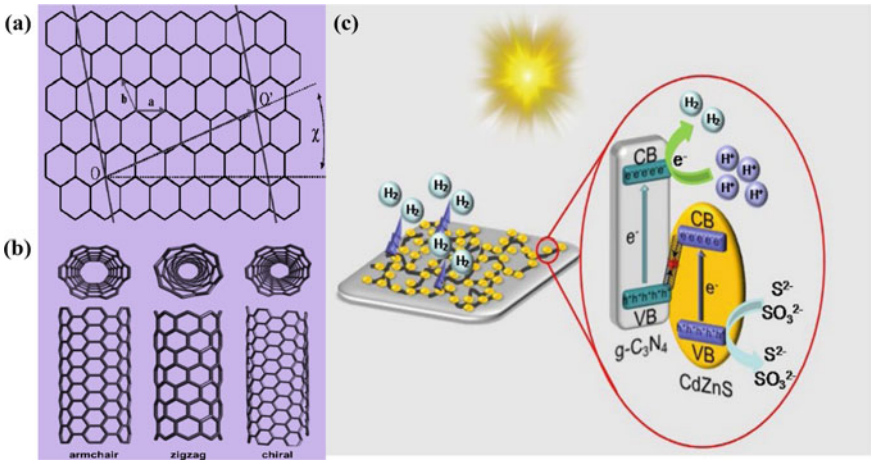

Fig. 7 **a** and **b** the formation of single-walled carbon nanotubes by rolling a graphene sheet along lattice vectors results in armchair, zigzag, and chiral tubes which are the three types of carbon nanotubes; **c** Proposed mechanism diagram of photocatalytic hydrogen production of Z-scheme g-C3N4/CNTs/CdZnS. "Reprinted with permission from Feng et al. [104]. Copyright 2021 Elsevier"

with a wide range of structural characteristics such as diameter, length, and chirality. The pure SWCNTs are visualized as tubular shell rolled of graphene sheet layered by benzene kind hexagonal rings of carbon atoms [92–94]

From these two different structures, it is possible for three different types of CNTs. They are armchair, zig-zag and chiral-type CNTs which are represented by indices of n and m. Therefore, when $n = m$ represents armchair, when $m = 0$ represents zig-zag and other configurations represent chiral nanotubes [95–99]. Figure 7a, b represents the types of SWCNTs. The diameter and chirality are calculated by the following equation [100]

$$D = a\left(n^2 + nm + m^2\right)^{1/2}/\pi$$

$$\theta = \tan^{-1}\left[3^{1/2}m/(m+2n)\right]$$

The circumference of SWCNTs has 10 atoms usually and tube thickness is one-atom-thick only, this nanotube have an aspect ratio of length- diameter was about 1000, so it can be nearly considered as one-dimensional structures [95]. SWCNTs have a diameter of ≈1 nm consisting of only one atomic sheet which can be visualized by rolled graphene (i.e. honeycomb structure sp^2 of carbon atom) sheet. The sp^2-bonded carbon materials give better mechanical properties [98]. The one-dimensional SWCNTs are attracted researcher to explore 1D physics in the quantum regimes and new optoelectronic devices. Moreover, the most prominent property in SWCNTs is charity-dependent metallicity. CNTs have high thermal conductivity (3000 W/m/K, comparable to diamond), good chemical and environmental stability. Along with these properties, the lightweight of carbon nanotubes makes them extremely promising for use in industries such as aerospace [101]. MWCNTs are sp^2 carbon made of elongated cylindrical nano-objects, and their diameter ranges from 3 to 30 nm, and they can grow to be several centimeters long, and therefore, their aspect ratio can range between ten and ten million. These MWCNTs can be distinguished from SWCNTs and double-wall carbon nanotubes. In MWCNTs, the wall thickness is constant along the axis; therefore, the inner channel is straight. A multi-walled carbon nanotube is made up of as many large molecules as the number of walls, and each molecule is as long as the nanotube itself. Carbon materials are mostly used as supporting materials for semiconductor photocatalysts. In addition, photocatalyst hydrogen (H_2) production was achieved by hybrid photocatalyst of semiconductor–carbon photocatalysts. The surface chemistry of carbon materials influences the interaction between semiconductor nanoparticles and carbon materials [102]. In this aspect, Wang et al. fabricated the MWCNTs as a supporting material of $Zn_xCd_{1-x}S$ nanoparticles by the solvothermal process, where $Zn(AC)_2{\cdot}2H_2O$, $CdCl_2{\cdot}2/5H_2O$ and thiourea were used as the precursor material to prepare $Zn_xCd_{1-x}S$. The average diameter of Zn0.83Cd0.17S nanoparticle was found ∼100 nm which was assembled on the surface of CNTs. Moreover, the combined $Zn_{0.83}Cd_{0.17}S$/CNTs nanocomposites give better dispersion and interfacial area. The excited photoelectron will move from the conduction band (CB) of $Zn_{0.83}Cd_{0.17}S$ to the surface of CNTs, resulting in the separation of photogenerated charge carriers at the interface between $Zn_{0.83}Cd_{0.17}S$ and CNTs. Under wavelength illumination ranging from 300 to 800 nm, the photocatalytic H_2 production rate of $Zn_{0.83}Cd_{0.17}S$/CNTs nanocomposite was 6.03 mmol h^{-1} g^{-1}, which was 1.5 times than that pure $Zn_{0.83}Cd_{0.17}S$ [103].

The MWCNTs/Pd-TiO_2 photocatalyst was tested for H_2 production under UV light which shows the production of H_2 as 25 mmol g^{-1} h^{-1}; this can be achieved due to electronic junction supporting the charge transfer between the MWCNTs-TiO_2. Moreover, the CNTS acts as a co-catalyst and excellently transfers the electron between Pd and TiO_2 [105]. Umer et al. investigated the montmorillonite (Mt) dispersed in single-wall carbon nanotubes (SWCNTs)/TiO_2 composite to produce photocatalytic H_2 evolution under visible light conditions. The SWCNTs-Mt (2–10 wt%)-doped TiO_2 produces H_2 volume of ca. 9780 ppm h^{-1} g^{-1}. To enhance the

separation efficiency of better absorption of visible light and photogenerated charge carriers are originated through synergic effect between Mt and SWCNTs. The co-doping between Mt and TiO_2 enhances the separation efficiency of electron/hole pairs [106]. As well as, CNT-Pt/TiO_2 photocatalysts prepared via hydrothermal and one-pot oxidation for production of photocatalytic hydrogen from glycerol and methanol from aqueous solutions. The H_2 production is increased by varying CNTs wt% in the range of 1–10 wt% loading with TiO_2 reported by Naffati et al. [107]. Moreover, this synergic effect enhances the separation of charge carriers and mobility in hybrid materials promoted by CNTs. The 1 wt% of CNTs with Pt/TiO_2 shows the highest photocatalytic H_2 production under UV-LED of (384 nm) irradiation. Although using methanol with this reaction produce H_2 of 2327 and 2091 μmol g^{-1} was obtained using glycerol. In this aspect, Peng et al. [108] synthesized MWCNTs/CdS (cadmium sulfide) by hydrothermal method. The 10 wt% of MWCNT with CdS derived from at 160 °C shows high photocatalytic hydrogen production efficiency due to its fastest carrier separation. In MWCNTs, the presence of carboxyl leads to good chemical bonding between MWCNTs and CdS nanoparticles which result in the synergic effect of CNTs and CdS. The binary MWCNTs/CdS nanocomposite is efficient under visible light-driven photocatalysts which shows better durability due to their good chemical bonding between composites of MWCNTs/CdS, which enhanced the separation efficiency and charge separation and its potential for the developing of efficient photocatalysts for H_2 production. Feng et al. [104] performed the photocatalysts hydrogen production on g-C_3N_4/CNTs/CdZnS which is shown in Fig. 7c. The CdZnS nanoparticles are compounded uniformly on the surface of g-C_3N_4/CNTs to form the heterojunctions which improve the photocatalytic H_2 production. Moreover, the mass ratio of 1:8 (g-C_3N_4/CNTs to CdZnS) displayed better performance on photocatalytic H_2 production of 28.74 mmol g^{-1} h^{-1}. Z-scheme heterojunctions improves the system separation efficiency and photogenerated carrier lifetime on these ternary nanocomposites, which can make better and continue to produce H_2 efficiently and stably.

3.2 2D Materials

The material's properties are impacted not only by its chemical bonding but also by its dimensions and shape at the mesoscopic scale. This is especially true in the case of carbon-based materials. Carbon possesses four valence electrons in its ground state, two in the 2s subshell and two in the 2p subshell. While establishing bonds between neighboring atoms of carbon, the transfers of one 2s electrons into the unoccupied 2p orbital take place and then create bonds with additional atoms through the orbit of sp hybridization. Depends on the number of p orbitals (one to three) mashing up with the s orbital the sp hybridization is categorized by three types which are sp, sp^2, and sp^3 hybridization. The hybridized carbon atoms in the form of sp^2 and sp^3 establish bonds with three and four carbon atoms, respectively. These carbon-based building blocks are known as two-dimensional (2D) materials which include graphene, graphitic

carbon nitride and graphdiyne. The arrangement of carbon atoms on a honeycomb lattice brought outstanding properties includes exceptional electronic, mechanical, and optical properties. Owing to its outstanding characteristics, two-dimensional (2D) materials have fascinated a lot of interdisciplinary research consideration in the field of energy and environmental applications. In that perspective, utilization of 2D materials for the generation of H_2 from the process of photocatalytic water splitting is the most idealistic method for gaining carbon-free fuel [109].

3.2.1 Graphene

The wonder material "graphene" was discovered in 2004 by Geim and Novoselov [110]. The discovery of graphene ushered in a new era of the materials world and is much recognized for its exceptional properties such as large surface area (2630 $m^2\ g^{-1}$), outstanding electronic mobility (200,000 $cm^2\ V^{-1}\ s^{-1}$), high thermal conductivity (3000 $W\ m^{-1}\ K^{-1}$) and robust mechanical strength (1060 GPa). Various physical methods have been tried to isolate a single-layer defect-free graphene sheet. Chemical vapour deposition (CVD), thermal exfoliation, solvent assisted exfoliation and ultrasonication are a few examples [111]. However, commercial implementation is hampered by expensive and time-consuming methods as well as the inability to produce big quantities. So chemical oxidation method is adopted to oxidize graphite by involving strong oxidizing agents for the formation of graphite oxide, and from this procedure, graphene oxide (GO) can be obtained easily through the repulsive forces acting between negatively charged sheets [112, 113]. The GO sheets can be partially diminished via hydrothermal, chemical, or thermal exfoliation methods to obtain reduced graphene oxide (rGO) [114]. Despite the fact that these techniques generate graphene sheets with few defects, their properties are identical to graphene. When graphite is oxidized to graphene oxide (GO), it becomes a semiconductor. The addition of various oxygen-carrying functions to graphene via oxidation converts some of the sp^2 carbons into sp^3 carbons, owing to the breaking of the p-conjugated system [115]. The carbon skeleton of GO turns positive due to the higher electronegativity of oxygen, and GO behaves as a p-type material [116]. The presence of both sp^2 (conducting) and sp^3 (non-conducting) carbons results in the formation of bandgap which exclusively depends on the degree of oxidation. The bandgap of GO can be controlled by adjusting the oxidation level. At first, the splitting of water into hydrogen and oxygen using GO was reported by Yeh et al. [69]. Depending on the oxidation level, the bandgap of GO was found to be 2.4–4.3 eV, and this bandgap was capable of meeting the water splitting threshold that is 1.23 V. After 6 h of visible light irradiation, the negative conduction band produced a hydrogen (H_2) yield of 280 μmol and then the yield of hydrogen increased to 17,000 μmol when methanol was used as a sacrificial donor. Furthermore, to improve the hydrogen evaluation rate, graphene oxide (GO) can be composited with other inorganic semiconducting materials. Owing to the negatively charged surface of GO, the inorganic nanomaterials were immobilized by attractive force acts between them. Additionally,

GO offers seamless nucleation sites for the growth of metal oxide semiconducting nanoparticles and also prevents them from agglomeration.

Graphene-Based Composites

TiO_2 is widely utilized in photocatalytic hydrogen generation from water splitting because of its inexpensiveness, lack of toxicity and great stability [117]. Zhang et al. [118] explored photocatalytic H_2 evolution of TiO_2/graphene sheets (GS). The results indicate the increase in H_2 production with increase in GS content (4.5 μmol h^{-1}–5.4 μmol h^{-1}), respectively. Shen et al. [119] demonstrated the superiority of TiO_2/rGO synthesized via one-step hydrothermal method, and the composite displayed a H_2 yield of 4.0 μmol h^{-1} under irradiation of UV–visible light. The increased activity of the composite may be due to interfacial transfer of electrons from TiO_2 to graphene which is assisted by the energy-level variations. Xiang et al. [120] prepared graphene-modified TiO_2 nanosheets through microwave-hydrothermal method and exhibits a H_2 yield of 736 μmol h^{-1} g^{-1} by an AQY of 3.1%. The high H_2 production may be ascribed to the composite material (TiO_2 modified graphene sheets) which acts as an electron acceptor and efficiently restricts the recombination rate of electron–hole pair. Lv et al. [121] demonstrated the fabrication of photocatalysts containing CdS or TiO_2 graphene composite by one-pot synthesis method, and hydrogen-generating ability of the photocatalysts was examined using sacrificial electron (SA) donors (Na_2S and Na_2SO_3). Min et al. [122] investigated the MoS_2 confined on RGO sheets attached with Eosin Y as SA in photocatalytic systems for H_2 evolution, and it exhibits a AQY of 24% under visible light irradiation (≥420 nm). Tran et al. [123] studied Cu_2O/rGO composite for hydrogen generation, and they tried to overcome the rapid deactivation of Cu_2O via photocorrosion phenomenon, which causes due to the redox reaction of Cu_2O to CuO and Cu. Khan et al. [124] investigated the significance of Al_2O_3/CdS/GO and ZnO/CdS/GO in H_2 evolution with SA (Na_2SO_3 and Na_2S) which displays an AQY of 14% and 30%. Mou et al. [125] prepared RuO_2/$TiSi_2$/graphene as photocatalyst for H_2 generation via water splitting. However, increasing the amount of RuO_2 on the surface of $TiSi_2$ resulted in charge recombination centres. Furthermore, similar action was found with addition of RGO, where 1% loading amount of RGO works as an enhanced charge transport and further increasing the loading, resulting in a decrease in H_2 evolution. Based on the discussion, graphene and graphene-based composites clearly act as an effective support for semiconducting photocatalysts, particularly for generating H_2 via water splitting. The importance of graphene and graphene-based composites in suppressing the recombination rate in single and dual semiconducting photocatalysts has received a lot of attention. Even though the performance of graphene-based photocatalysts in water splitting is critical, graphene's high production cost delays the commercialization process.

3.2.2 Graphitic Carbon Nitride

As another type of layered 2D material is graphitic-phase carbon nitride (g-C_3N_4) which sparked lot of curiosity among scientists because of its unique structure and interesting characteristics. Since it discovered in 1834, carbon nitride (C_3N_4) has been considered as ace of the earliest organic conjugated polymers which has five phase classifications together with α, β, cubic, pseudocubic and graphitic phase. Specifically, g-C_3N_4 is made up of layers of 2D conjugated structures with s-triazine or tri-s-triazine subunits linked by tertiary amines. Thermal polycondensation (Fig. 8a) is used to make g-C_3N_4 from low-cost carbon-based precursors which contains nitrogen urea, cyanamide, thiourea, melamine and dicyanamide. Initially, Biureate is formed when it dimerizes and then it cyclizes to cynauric acid, which combines with the ammonia gas to produce ammelide and melamine during pyrolysis. The graphite-like planer architecture with p-conjugated systems allows charge carriers to be transported, whereas the bandgap of 2.7 eV allows it to work in the visible region of the solar spectrum at approximately 460 nm. The benefits of g-C_3N_4 consist of visible light responsive, better thermal stability in ambient conditions, good chemical resistivity and eco-friendly. Furthermore, the electronic band position of the negative conduction band (CB) is higher than H^+/H_2 and the positive valence band (VB) superior than H_2O/O_2 drives the g-C_3N_4 specifically in the H_2 production from the solar-driven water splitting process [126, 127]. Hong et al. [128] prepared g-C_3N_4 nanosheets by directly thermal calcination method using an optimized hydrothermally treated melamine as precursor. The resulting nanosheets had outstanding visible light-driven photocatalytic water splitting capability of 503 mol h^{-1} g^{-1} hydrogen evolution (Fig. 8b). One of the initial efforts by Wang et al. [129] reveals the usage of g-C_3N_4 to yield H_2 by water splitting process in the presence of triethanolamine which generated 0.1–4.0 μmoles/h under the irradiation source of visible light. Upon the addition of co-catalyst (3% Pt), the yield of H_2 was increased by further 10–15%. However, its photocatalytic activity is limited by its lower electrical conductivity, higher recombination rate, and poor light absorption. Several approaches were indeed made to enhance the photocatalytic activity g-C_3N_4 which are doping, tailoring the nanoarchitecture, incorporation of noble metal, development of heterojunctions with other photoactive materials.

The g-C3N4 catalyst based on heterojunctions has received a lot of attention because of its synergistic behaviour. So, using the impregnation and chemical reduction method, the nanocomposites of g-C_3N_4 and graphene oxide (GO) were synthesized by thermally treating melamine and GO at 550 °C in inert environment [130]. In this context, graphene served as conductive pathways, allowing the charge carriers to be effectively separated. So, the graphene/g-C_3N_4 nanocomposite displays a H_2 production of 451 μmol h^{-1}, which the pure g-C_3N_4 possess 3.07 times lesser. Song et al. reported that their prepared rGO/g-C_3N_4 via a simple hydrothermal reduction method yields a H_2 production rate of around 55.8 μmol h^{-1} g^{-1} [131]. To increase the photoactivity of g-C_3N_4, Zou et al. [132] created a nanocomposite of N-GQDs/g-C_3N_4 using a simple method. Because of the various functions served by the N-GQDs, this nanocomposite demonstrated enhanced activity in photocatalytic H_2

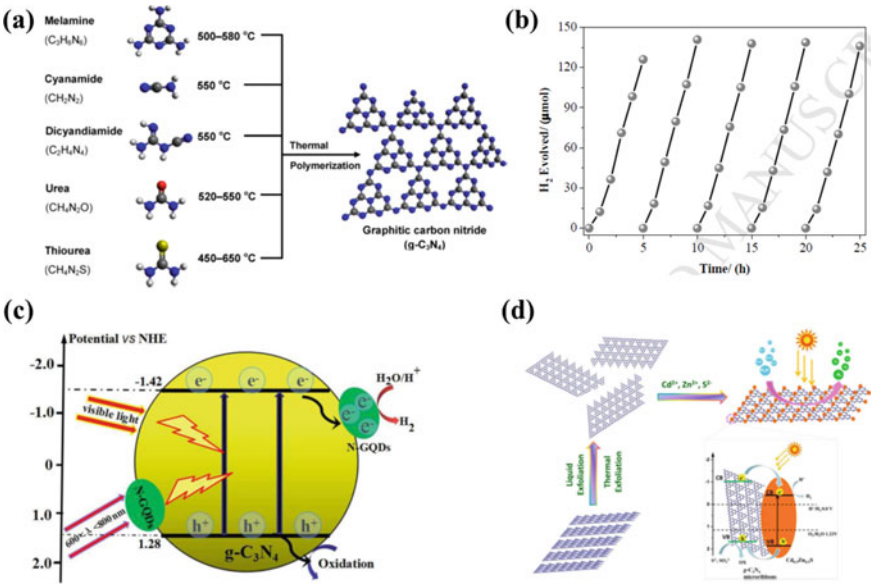

Fig. 8 **a** The synthesis of g-C_3N_4 by thermal polymerization of various precursors is depicted schematically. "Reprinted with permission from Ong et al. [138]. Copyright 2016 American Chemical Society." **b** Stability test of hydrogen production over the g-C_3N_4 nanosheets. g-C_3N_4. "Reprinted with permission from Hong et al. [128]. Copyright 2017 Elsevier." **c** Mechanism for H_2 evolution by using N-GQDs/CN-U. "Reprinted with permission from Zou et al. [132]. Copyright 2016 Elsevier." **d** The synthesis of $Cd_{0.5}Zn_{0.5}S@C_3N_4$ and visible light-driven H_2 production are depicted schematically. "Reprinted with permission from Yao et al. [135]. Copyright 2016 Elsevier"

evolution of around 43.6 mol h^{-1} that would have been 2.16 times larger compared to pure g-C_3N_4. Figure 8c illustrates the photocatalytic H_2 evolution pathway in N-GQDs/g-C_3N_4. As per the suggested mechanism, g-C_3N_4 absorbs in the region (420–470 nm) and results in production of charge carriers. On the contrary, absorbed light at 600–800 nm by g-C_3N_4 generates electron and hole. As a result, electrons from the conduction band of g-C_3N_4 migrated to the edge of N-GQDs and those electrons are having ample time to convert H_2O to H_2 because of its effective separation of charge carrier. Another approach has been reported by utilizing ZIF-8/g-C_3N_4 prepared by simple thermal condensation method which exhibits a H_2 evolution 32.6 μmol h^{-1} that was 36.2 times higher compared to bare g-C_3N_4 [133]. Wang et al. [134] reported the integration of silicon carbide (SiC) with g-C_3N_4 for the first time. The composite had a high photoactivity and a rate of H^2 generation of 182 mol h^{-1} that was 3.4 times higher than the pure g-C_3N_4. The band edges of SiC and g-C_3N_4 matched appropriately to generate a heterojunction photocatalyst with better electron–hole separation.

Yao et al. proposed a Type-II photocatalyst with excellent efficiency composed of 2D g-C_3N_4 micronanoribbons and $Cd_{0.5}Zn_{0.5}S$ quantum dots Fig. 8d [135]. The authors integrated the virtues of nanostructure engineering based on the benefits

of Type-II structures. The composite displays the maximum H_2 generation rate of 33.41 mmol h^{-1} g^{-1} and an AQY of 46.65% at visible light irradiation (450 nm). In g-C_3N_4-based Z-scheme systems, the narrow bandgap oxides have fascinating potentials throughout the evolution of O_2 in water splitting process. She et al. [136] demonstrated that a 2D hybrid made up of g-C_3N_4 nanosheets and Fe_2O_3 nanosheets coupled with a tight interface may be used to build a direct Z-scheme all-solid-state system for photocatalytic water splitting process. The composite showed an excellent hydrogen evolution rate of 30 mmol g^{-1} h^{-1} and an AQY of 44.35% under the irradiation of visible light (420 nm). Similarly, in order to achieve optimal performance, the main factors that have a substantial impact on water splitting efficiency must be optimized are: type and concentration of redox mediator, the pH value of the reaction medium and the weight per cent between two photocatalysts. Tang et al. prepared the combination of $BiVO_4$ and WO_3 with g-C_3N_4 to form a Z-scheme system with taking the above factors into account. Under ideal condition, g-C_3N_4/WO_3 (I/IO_3 as a redox mediator) exhibits a H_2 and O_2 evolution of 36 and 18 mol g^{-1} h^{-1}, while for g-C_3N_4/$BiVO_4$ the corresponding evolutions are 21.2 and 11.0 μmol g^{-1} h^{-1} by using $Fe^{2+/3+}$ as a redox mediator [137].

Moreover, the intriguing metal-free structure and high physicochemical stability of g-C_3N_4 materials offer both technical potential and mechanistic vision into the water splitting mechanism. By modifying the exterior construction of g-C_3N_4 built on strategies like Type-I and Z-scheme deliberately improves the efficiency and durability in mutual of hydrogen evolution half reaction and overall water splitting process.

4 Conclusion

The advantages of carbonaceous based (0D, 1D and 2D) nanostructures composites in photocatalytic water splitting were emphasized in this chapter. These carbonaceous nanostructure materials revealed to have strong carrier transport and electron accepting capabilities, which are the most important qualities for increasing hydrogen generation efficiency by increasing the visible light absorption. In addition, the carbonaceous nanostructured-based semiconductor photocatalytic materials enhance the hydrogen evolution efficiency and displayed outstanding stability, where the integration of semiconducting materials established the effective transfer of an electron between the heterostructures and efficient separation of charge carriers. Also, the photocatalytic semiconductors act as an efficient light adsorber and electron acceptor which enhance the overall efficiency of water splitting. In conclusion, carbon-based nanostructures have a great potential in water splitting application as photocatalytic hydrogen generation.

References

1. Sadanandam G, Lalitha K, Kumari VD, Shankar MV, Subrahmanyam M (2013) Cobalt doped TiO2: a stable and efficient photocatalyst for continuous hydrogen production from glycerol: water mixtures under solar light irradiation. Inter J Hydr Energ 23:9655–9664
2. Kumar DP, Reddy NL, Srinivas B, Durgakumari V, Roddatis V, Bondarchuk O, Karthik M, Ikuma Y, Shankar MV (2016) Stable and active CuxO/TiO_2 nanostructured catalyst for proficient hydrogen production under solar light irradiation. Sol Energ Mater and Sol Cells 46:63–71
3. Asahi RY, Morikawa TA, Ohwaki T, Aoki K, Taga Y (2001) Visible-light photocatalysis in nitrogen-doped titanium oxides. Science 293:269–271
4. Kudo A, Miseki Y (2009) Heterogeneous photocatalyst materials for water splitting. Chem Soc Rev 38:253–278
5. Barber J et al (2009) Photosynthetic energy conversion: natural and artificial. Chem Soc Rev 38:185–196
6. Fujishima A, Honda K (1972) Electrochemical photolysis of water at a semiconductor electrode. Nature 238:37–38
7. Li X, Yu J, Low J, Fang Y, Xiao J, Chen X (2015) Engineering heterogeneous semiconductors for solar water splitting. J Mat Chem A 6:2485–2534
8. Xiang Q, Yu J, Jaroniec M (2012) Graphene-based semiconductor photocatalysts. Chem Soc Rev 41:782–796
9. Kang ZC, Wang ZL (1997) Chemical activities of graphitic carbon spheres. J Mole Cat A: Chem 118:215–222
10. Park C, Engel ES, Crowe A, Gilbert TR, Rodriguez NM (2000) Use of carbon nanofibers in the removal of organic solvents from water. Lang 21:8050–8056
11. Du J, Liu Z, Li Z, Han B, Sun Z, Huang Y (2005) Carbon onions synthesized via thermal reduction of glycerin with magnesium. Mater Chem and Phy 93:178–180
12. Rana RK, Gedanken A (2002) Carbon nanoflask: a mechanistic elucidation of its formation. J Phy Chem B 38:9769–9776
13. Ugrate D et al (1992) Curling and closure of graphitic networks under electron beam irradiation. Nature 359:707–709
14. Jin YZ, Gao C, Hsu WK, Zhu Y, Huczko A, Bystrzejewski M, Roe M, Lee CY, Acquah S, Kroto H, Walton DR (2005) Large-scale synthesis and characterization of carbon spheres prepared by direct pyrolysis of hydrocarbons. Carbon 43(9):1944–1953
15. Wang ZL, Yin JS (1998) Graphitic hollow carbon calabashes. Chem Phy Lett 289:189–192
16. Geim AK, Novoselov KS (2010) The rise of grapheme. In: Nanoscience and technology: a collection of reviews from nature journals, pp 11–19
17. Rao CE, Sood AE, Subrahmanyam KE, Govindaraj A (2009) Graphene: the new two-dimensional nanomaterial. Ang Chem Inter Edit 42:7752–7777
18. Jun LY, Mubarak NM, Yee MJ, Yon LS, Bing CH, Khalid M, Abdullah EC (2018) An overview of functionalised carbon nanomaterial for organic pollutant removal. J Ind Eng Chem 67:175–186
19. Ma Y, Wang X, Jia Y, Chen X, Han H, Li C (2014) Titanium dioxide-based nanomaterials for photocatalytic fuel generations. Chem Rev 19:9987–10043
20. Bera R, Dutta A, Kundu S, Polshettiwar V, Patra A (2018) Design of a CdS/CdSe heterostructure for efficient H_2 generation and photovoltaic applications. J Phy Chem C 23:12158–12167
21. Chen H, Liu XY, Wang S, Wang X, Wei Q, Jiang X, Wang F, Xu K, Ke J, Zhang Q, Gao Q (2018) Quaternary two dimensional Zn–Ag–In–S nanosheets for highly efficient photocatalytic hydrogen generation. J Mat Chem A 25:11670–11675
22. Wu MC, Wu PY, Lin TH, Lin TF (2018) Photocatalytic performance of Cu-doped TiO_2 nanofibers treated by the hydrothermal synthesis and air-thermal treatment. Appl Sur Sci 430:390–398

23. Ma L, Chen YL, Yang DJ, Li HX, Ding SJ, Xiong L, Qin PL, Chen XB (2020) Multi-interfacial plasmon coupling in multigap (Au/AgAu)@ CdS core–shell hybrids for efficient photocatalytic hydrogen generation. Nanosc 7:4383–4392
24. Shahzad K, Tahir MB, Sagir M (2019) Engineering the performance of heterogeneous WO_3/fullerene@ Ni_3B/Ni $(OH)_2$ photocatalysts for hydrogen generation. Intern J Hydro Energ 39:21738–21745
25. Li J, Zhang L, Li J, An P, Hou Y, Zhang J (2019) Nanoconfined growth of carbon-encapsulated cobalts as cocatalysts for photocatalytic hydrogen evolution. ACS Sustain Chem Eng 16:14023–14030
26. Patra KK, Ghosalya MK, Bajpai H, Raj S, Gopinath CS (2019) Oxidative disproportionation of MoS_2/GO to MoS_2/MoO_3–x/RGO: integrated and plasmonic 2D-multifunctional nanocomposites for solar hydrogen generation from near-infrared and visible regions. J Phy Chem C 35:21685–21693
27. Rajaambal S, Sivaranjani K, Gopinath CS (2015) Recent developments in solar H_2 generation from water splitting. J Chem Sci 127(1):33–47
28. Du J, Li S, Du Z, Meng S, Li B (2021) Boron/oxygen-codoped graphitic carbon nitride nanomesh for efficient photocatalytic hydrogen evolution. Chem Eng J 407:127114
29. Jinbo P, Sheng S, Wei Z, Jie T, Hongzhi D, Jinbo W, Lang C, Chak-Tong A, Shuang-Feng Y (2020) Recent progress in photocatalytic hydrogen evolution. Acta Phy-Chim Sin 36(3):1905068
30. San Martín S, Rivero MJ, Ortiz I (2020) Unravelling the mechanisms that drive the performance of photocatalytic hydrogen production. Catalysts 10(8):901
31. Huang Z, Xi L, Subhani Q, Yan W, Guo W, Zhu Y (2013) Covalent functionalization of multi-walled carbon nanotubes with quaternary ammonium groups and its application in ion chromatography. Carbon 62:127–134
32. Mallakpour S, Soltanian S (2016) Surface functionalization of carbon nanotubes: fabrication and applications. RSC Adv 6:109916–109935
33. Toma FM, Sartorel A, Iurlo M, Carraro M, Rapino S, Hoober-Burkhardt L, Da Ros T, Marcaccio M, Scorrano G, Paolucci F, Bonchio M (2011) Tailored functionalization of carbon nanotubes for electrocatalytic water splitting and sustainable energy applications. Chemsuschem 4:1447
34. Zheng XT, Ananthanarayanan A, Luo KQ, Chen P (2015) Glowing graphene quantum dots and carbon dots: properties, syntheses, and biological applications. Small 14:1620–1636
35. Tian P, Tang L, Teng KS, Lau SP (2018) Graphene quantum dots from chemistry to applications. Mater Today Chem 10:221–258
36. Ge J, Zhang Y, Park SJ (2019) Recent advances in carbonaceous photocatalysts with enhanced photocatalytic performances: a mini review. Materials 12:1916
37. Gao J, Zhu M, Huang H, Liu Y, Kang Z (2017) Advances, challenges and promises of carbon dots. Inorg Chem Front 12:1963–1986
38. Mehta A, Mishra A, Basu S, Shetti NP, Reddy KR, Saleh TA, Aminabhavi TM (2019) Band gap tuning and surface modification of carbon dots for sustainable environmental remediation and photocatalytic hydrogen production–a review. J Environ Manage 250:109486
39. Xu X, Ray R, Gu Y, Ploehn HJ, Gearheart L, Raker K, Scrivens WA (2004) Electrophoretic analysis and purification of fluorescent single-walled carbon nanotube fragments. J Am Chem Soc 126(40):12736–12737
40. Ali H, Ghosh S, Jana NR (2020) Fluorescent carbon dots as intracellular imaging probes. Wiley Interdisci Rev: Nanomed Nanobiotec 4:1617
41. Reckmeier CJ, Schneider J, Susha AS, Rogach AL (2016) Luminescent colloidal carbon dots: optical properties and effects of doping. Opt Express 24:312–340
42. Luo H, Guo Q, Szilágyi PÁ, Jorge AB, Titirici MM (2020) Carbon dots in solar-to-hydrogen conversion. Trends in Chemistry 2:623–637
43. Rao VN, Reddy NL, Kumari MM, Cheralathan KK, Ravi P, Sathish M, Neppolian B, Reddy KR, Shetti NP, Prathap P, Aminabhavi TM (2019) Sustainable hydrogen production for the greener environment by quantum dots-based efficient photocatalysts: a review. J Environ Manag 248:109246

44. Wang Y, Zhu Y, Yu S, Jiang C (2017) Fluorescent carbon dots: rational synthesis, tunable optical properties and analytical applications. RSC Adv 65:40973–40989
45. Tang Y, Hao R, Fu Y, Jiang Y, Zhang X, Pan Q, Jiang B (2016) Carbon quantum dot/mixed crystal TiO_2 composites via a hydrogenation process: an efficient photocatalyst for the hydrogen evolution reaction. RSC Adv 99:96803–96808
46. Reddy NR, Bhargav U, Kumari MM, Cheralathan KK, Sakar M (2020) Review on the interface engineering in the carbonaceous titania for the improved photocatalytic hydrogen production. Int J Hydrogen Energ 45(13):7584–75615
47. Tian P, Tang L, Teng KS, Lau SP (2018) Materials Today Chemistry 10:221e258
48. Shen J, Zhu Y, Yang X, Li C (2012) Graphene quantum dots: emergent nanolights for bioimaging, sensors, catalysis and photovoltaic devices. Chem comm 31:3686–3699
49. Gliniak J, Lin JH, Chen YT, Li CR, Jokar E, Chang CH, Peng CS, Lin JN, Lien WH, Tsai HM, Wu TK (2017) Sulfur-doped graphene oxide quantum dots as photocatalysts for hydrogen generation in the aqueous phase. Chemsuschem 16:3260–3267
50. Titirici MM, White RJ, Brun N, Budarin VL, Su DS, del Monte F, Clark JH, MacLachlan MJ (2015) Sustainable carbon materials. Chem Soc Rev 44(1):250–290
51. Kang Z, Liu Y, Gao J, Zhu M (2017) Carbon dots for environmental and energy applications: advances, challenges and promises. Inorg Chem Front 4:1963–1986
52. Jiao Y, Huang Q, Wang J, He Z, Li Z (2019) A novel MoS_2 quantum dots (QDs) decorated Z-scheme g-C3N4 nanosheet/N-doped carbon dots heterostructure photocatalyst for photocatalytic hydrogen evolution. Appl Cat B: Environ 247:124–132
53. Sui Y, Wu L, Zhong S, Liu Q (2019) Carbon quantum dots/TiO_2 nanosheets with dominant (001) facets for enhanced photocatalytic hydrogen evolution. Appl Surf Sci 480:810–816
54. Shi W, Guo F, Li M, Shi Y, Tang Y (2019) N-doped carbon dots/CdS hybrid photocatalyst that responds to visible/near-infrared light irradiation for enhanced photocatalytic hydrogen production. Sep Purif Tech 212:142–149
55. Gultom NS, Abdullah H, Kuo DH (2019) Effects of graphene oxide and sacrificial reagent for highly efficient hydrogen production with the costless Zn (O, S) photocatalyst. Int J Hydrogen Energ 56:29516–29528
56. Sumana K, Vijayamohanan KP (2020) Synthesis and characterization of graphene quantum dots. Phy Sci Rev 5:20190013
57. Nguyen BS, Xiao YK, Shih CY, Nguyen VC, Chou WY, Teng H (2018) Electronic structure manipulation of graphene dots for effective hydrogen evolution from photocatalytic water decomposition. Nanos 22:10721–10730
58. Sk MA, Ananthanarayanan A, Huang L, Lim KH, Chen P (2014) Revealing the tunable photoluminescence properties of graphene quantum dots. J Mater Chem C 34:6954–6960
59. Ye R, Xiang C, Lin J, Peng Z, Huang K, Yan Z, Cook NP, Samuel EL, Hwang CC, Ruan G, Ceriotti G (2013) Coal as an abundant source of graphene quantum dots. Nat comm 1:1–7
60. Yan Y, Chen J, Li N, Tian J, Li K, Jiang J, Liu J, Tian Q, Chen P (2018) Systematic bandgap engineering of graphene quantum dots and applications for photocatalytic water splitting and CO_2 reduction. ACS Nano 4:3523–3532
61. Fantuzzi P, Candini A, Chen Q, Yao X, Dumslaff T, Mishra N, Coletti C, Müllen K, Narita A, Affronte M (2019) Color sensitive response of graphene/graphene quantum dot phototransistors. J Phys Chem C 43:26490–26497
62. Tian P, Tang L, Teng KS, Lau SP (2018) Graphene quantum dots from chemistry to applications. Mat Today Chem 10:221–258
63. Zhang R, Qi S, Jia J, Torre B, Zeng H, Wu H, Xu X (2015) Size and refinement edge-shape effects of graphene quantum dots on UV–visible absorption. J Alloy Compd 623:186–191
64. Raghavan A, Sarkar S, Nagappagari LR, Bojja S, MuthukondaVenkatakrishnan S, Ghosh S (2020) decoration of graphene quantum dots on TiO_2 nanostructures: photosensitizer and cocatalyst role for enhanced hydrogen generation. Indus Eng Chem Res 29:13060–13068
65. Calabro RL, Yang DS, Kim DY (2019) Controlled nitrogen doping of graphene quantum dots through laser ablation in aqueous solutions for photoluminescence and electrocatalytic applications. ACS Appl Nano Mater 11:6948–6959

66. Zhang Z, Zhang J, Chen N, Qu L (2012) Graphene quantum dots: an emerging material for energy-related applications and beyond. Energ Environ Sci 10:8869–8890
67. Li X, Shen R, Ma S, Chen X, Xie J (2018) Graphene-based heterojunction photocatalysts. Appl Surf Sci 430:53–107
68. Yeh TF, Teng CY, Chen SJ, Teng H (2014) Nitrogen-doped graphene oxide quantum dots as photocatalysts for overall water-splitting under visible light Illumination. Adv Mater 20:3297–3303
69. Yeh TF, Syu JM, Cheng C, Chang TH, Teng H (2010) Graphite oxide as a photocatalyst for hydrogen production from water. Adv Funct Mater 14:2255–2262
70. Xie G, Zhang K, Guo B, Liu Q, Fang L, Gong JR (2013) Graphene-based materials for hydrogen generation from light-driven water splitting. Adv Mater 28:3820–3839
71. Yeh TF, Chen SJ, Teng H (2015) Synergistic effect of oxygen and nitrogen functionalities for graphene-based quantum dots used in photocatalytic H_2 production from water decomposition. Nano Energ 12:476–485
72. Chen LC, Teng CY, Lin CY, Chang HY, Chen SJ, Teng H (2016) Architecting nitrogen functionalities on graphene oxide photocatalysts for boosting hydrogen production in water decomposition process. Adv Energ Mater 22:1600719
73. Tian H, Shen K, Hu X, Qiao L, Zheng WN (2017) S co-doped graphene quantum dots-graphene-TiO_2 nanotubes composite with enhanced photocatalytic activity. J Alloy Compd 691:369–377
74. Qu A, Xie H, Xu X, Zhang Y, Wen S, Cui Y (2016) High quantum yield graphene quantum dots decorated TiO_2 nanotubes for enhancing photocatalytic activity. Appl Surf Sci 375:230–241
75. Sudhagar P, Herraiz-Cardona I, Park H, Song T, Noh SH, Gimenez S, Sero IM, Fabregat-Santiago F, Bisquert J, Terashima C, Paik U (2016) Exploring graphene quantum dots/TiO_2 interface in photoelectrochemical reactions: solar to fuel conversion. Electro Act 187:249–255
76. Ebrahimi M, Samadi M, Yousefzadeh S, Soltani M, Rahimi A, Chou TC, Chen LC, Chen KH, Moshfegh AZ (2017) Improved solar-driven photocatalytic activity of hybrid graphene quantum dots/ZnO nanowires: a direct Z-scheme mechanism. ACS Sustain Chem Eng 1:367–375
77. Lei Y, Yang C, Hou J, Wang F, Min S, Ma X, Jin Z, Xu J, Lu G, Huang KW (2017) Strongly coupled CdS/graphene quantum dots nanohybrids for highly efficient photocatalytic hydrogen evolution: unraveling the essential roles of graphene quantum dots. Appl Cat B: Environ 216:59–69
78. Dinda D, Park H, Lee HJ, Oh S, Park SY (2020) Graphene quantum dot with covalently linked Rhodamine dye: a high efficiency photocatalyst for hydrogen evolution. Carbon 167:760–769
79. Yu S, Zhong YQ, Yu BQ, Cai SY, Wu LZ, Zhou Y (2016) Graphene quantum dots to enhance the photocatalytic hydrogen evolution efficiency of anatase TiO_2 with exposed {001} facet. Phy Chem Chem Phy 30:20338–20344
80. Ahmad I, Akhtar MS, Ahmed E, Ahmad M, Naz MY (2021) Lu modified ZnO/CNTs composite: a promising photocatalyst for hydrogen evolution under visible light illumination. J Colloid Interface Sci 584:182–192
81. Chu J, Han X, Yu Z, Du Y, Song B, Xu P (2018) Highly efficient visible-light-driven photocatalytic hydrogen production on CdS/Cu_7S_4/g-C_3N_4 ternary heterostructures. ACS Appl Mater Interface 10:20404–20411
82. Vu MH, Sakar M, Nguyen CC, Do TO (2018) Chemically bonded Ni cocatalyst onto the S doped g-C_3N_4 nanosheets and their synergistic enhancement in H_2 production under sunlight irradiation. ACS Sustain Chem Eng 6:4194–4203
83. You Y, Wang S, Xiao K, Ma T, Zhang Y, Huang H (2018) Z-scheme g-C_3N_4/Bi_4NbO_8Cl heterojunction for enhanced photocatalytic hydrogen production. ACS Sustain Chem Eng 6:16219–16227
84. Yang R, Song K, He J, Fan Y, Zhu R (2019) Photocatalytic hydrogen production by RGO/$ZnIn_2S_4$ under visible light with simultaneous organic amine degradation. ACS Omega 4:11135–11140

85. Hao X, Jin Z, Yang H, Lu G, Bi Y (2017) Peculiar synergetic effect of MoS_2 quantum dots and graphene on metal-organic frameworks for photocatalytic hydrogen evolution. Appl Catal B: Environ 210:45–56
86. Iijima S et al (1991) Helical microtubules of graphitic carbon. Nature 354:56–58
87. Liang X, Zeng M, Qi C (2010) One-step synthesis of carbon functionalized with sulfonic acid groups using hydrothermal carbonization. Carbon 6:1844–1848
88. Zhang WD, Xu B, Jiang L (2010) Functional hybrid materials based on carbon nanotubes and metal oxides. J Mater Chem 31:6383–6391
89. Liu Z, Chen K, Davis C, Sherlock S, Cao Q, Chen X, Dai H (2008) Drug delivery with carbon nanotubes for in vivo cancer treatment. Canc Res 16:6652–6660
90. Xiao S, Zhu W, Liu P, Liu F, Dai W, Zhang D, Chen W, Li H (2016) CNTs threaded (001) exposed TiO_2 with high activity in photocatalytic NO oxidation. Nanoscale 5:2899–2907
91. Dai K, Zhang X, Fan K, Zeng P, Peng T (2014) Multiwalled carbon nanotube-TiO_2 nanocomposite for visible-light-induced photocatalytic hydrogen evolution. J Nanomat
92. Abrahamson J, Wiles PG, Rhoades BL (1999) Structure of carbon fibres found on carbon arc anodes. Carbon (New York, NY). 11:1873–1874
93. Hirlekar R, Yamagar M, Garse H, Vij M, Kadam V (2009) Carbon nanotubes and its applications: a review. Asian J Pharma Clin Res 4:17–27
94. Meyyappan M, Delzeit L, Cassell A, Hash D (2003) Carbon nanotube growth by PECVD: a review. Plasma Sources Sci Technol 2:205
95. Dresselhaus MS, Dresselhaus G, Jorio A (2004) Unusual properties and structure of carbon nanotubes. Annu Rev Mater Res 34:247–278
96. Terrones M et al (2003) Science and technology of the twenty-first century: synthesis, properties, and applications of carbon nanotubes. Annual Rev Mater Res 1:419–501
97. Zhang M, Li J (2009) Carbon nanotube in different shapes. Materials Today 6:12–18
98. Saifuddin N, Raziah AZ, Junizah AR (2013) Carbon nanotubes: a review on structure and their interaction with proteins. J Chem
99. Wang CY, Zhang YY, Wang CM, Tan VBC (2007) Buckling of carbon nanotubes: a literature survey. J Nanosci Nanotech 7(12):4221–4247
100. Yang Z, Ren J, Zhang Z, Chen X, Guan G, Qiu L, Zhang Y, Peng H (2015) Recent advancement of nanostructured carbon for energy applications. Chem Rev 11:5159–5223
101. Kim YA, Hayashi T, Endo M, Dresselhaus MS (2013) Carbon nanofibers. In: Springer handbook of nanomaterials, Springer, pp 233–262
102. Vajtai R et al (2013) Springer handbook of nanomaterials. Springer Science & Business Media
103. Wang L, Yao Z, Jia F, Chen B, Jiang Z (2013) A facile synthesis of Zn_x Cd_{1-x} S/CNTs nanocomposite photocatalyst for H_2 production. Dalton Trans 27:9976–9981
104. Feng C, Chen Z, Jing J, Sun M, Tian J, Lu G, Ma L, Li X, Hou J (2021) Significantly enhanced photocatalytic hydrogen production performance of g-C_3N_4/CNTs/CdZnS with carbon nanotubes as the electron mediators. J Mater Sci Tech 80:75–83
105. Cao S, Yu J (2016) Carbon-based H_2-production photocatalytic materials. J Photochem Photob C: Photochem Rev 1(27):72–99
106. Umer M, Tahir M, Azam MU, Tahir B, Jaffar MM, Alias H (2019) Montmorillonite dispersed single wall carbon nanotubes (SWCNTs)/TiO_2 heterojunction composite for enhanced dynamic photocatalytic H_2 production under visible light. Appl Cla Sci 174:110–119
107. Naffati N, Sampaio MJ, Da Silva ES, Nsib MF, Arfaoui Y, Houas A, Faria JL, Silva CG (2020) Carbon-nanotube/TiO_2 materials synthesized by a one-pot oxidation/hydrothermal route for the photocatalytic production of hydrogen from biomass derivatives. Mat Sci Semic Proc 115:105098
108. Peng T, Zeng P, Ke D, Liu X, Zhang X (2011) Hydrothermal preparation of multiwalled carbon nanotubes (MWCNTs)/CdS nanocomposite and its efficient photocatalytic hydrogen production under visible light irradiation. Energy Fuels 5:2203–2210
109. Kumar P, Boukherroub R, Shankar K (2018) Sunlight-driven water-splitting using two-dimensional carbon based semiconductors. J Mater Chem A 27:12876–12931
110. Savage N et al (2012) Materials science: super carbon. Nature 483:S30–S31

111. Dikin DA, Stankovich S, Zimney EJ, Piner RD, Dommett GH, Evmenenko G, Nguyen ST, Ruoff RS (2007) Preparation and characterization of graphene oxide paper. Nature 448:457–460
112. Hummers WS Jr, Offeman RE (1958) Preparation of graphitic oxide. J Amer Chem Soc 6:1339–1339
113. Marcano DC, Kosynkin DV, Berlin JM, Sinitskii A, Sun Z, Slesarev A, Alemany LB, Lu W, Tour JM (2010) Improved synthesis of graphene oxide. ACS Nano 8:4806–4814
114. Zhu Y, Murali S, Cai W, Li X, Suk JW, Potts JR, Ruoff RS (2010) Graphene and graphene oxide: synthesis, properties, and applications. Adv Mater 35:3906–3924
115. Eda G, Mattevi C, Yamaguchi H, Kim H, Chhowalla M (2009) Insulator to semimetal transition in graphene oxide. J Phy Chem C 35:15768–15771
116. Eda G, Fanchini G, Chhowalla M (2008) Large-area ultrathin films of reduced graphene oxide as a transparent and flexible electronic material. Nat Nanotechnol 5:270–274
117. Nowotny J, Bak T, Nowotny MK, Sheppard LR (2007) Titanium dioxide for solar-hydrogen I. Functional properties. Int J Hydrogen Energ 32(14):2609–2629
118. Zhang X, Sun Y, Cui X, Jiang Z (2012) A green and facile synthesis of TiO_2/graphene nanocomposites and their photocatalytic activity for hydrogen evolution. Int J Hydrogen Energ 37:811–815
119. Shen J, Yan B, Shi M, Ma H, Li N, Ye M (2011) One step hydrothermal synthesis of TiO_2-reduced graphene oxide sheets. J Mater Chem 21:3415–3421
120. Xiang Q, Yu J, Jaroniec M (2011) Enhanced photocatalytic H_2-production activity of graphene-modified titania nanosheets. Nanoscale 9:3670–3678
121. Lv XJ, Fu WF, Chang HX, Zhang H, Cheng JS, Zhang GJ, Song Y, Hu CY, Li JH (2012) Hydrogen evolution from water using semiconductor nanoparticle/graphene composite photocatalysts without noble metals. J Mater Chem 22:1539–1546
122. Min S, Lu G (2012) Sites for high efficient photocatalytic hydrogen evolution on a limited-layered MoS_2 cocatalyst confined on graphene sheets-the role of grapheme. J Phy Chem C 116:25415–25424
123. Tran PD, Batabyal SK, Pramana SS, Barber J, Wong LH, Loo SCJ (2012) A cuprous oxide–reduced graphene oxide (Cu_2O–rGO) composite photocatalyst for hydrogen generation: employing rGO as an electron acceptor to enhance the photocatalytic activity and stability of Cu_2O. Nanoscale 4:3875–3878
124. Khan Z, Chetia TR, Vardhaman AK, Barpuzary D, Sastri CV, Qureshi M (2012) Visible light assisted photocatalytic hydrogen generation and organic dye degradation by CdS-metal oxide hybrids in presence of graphene oxide. RSC Adv 2:12122e8
125. Mou Z, Yin S, Zhu M, Du Y, Wang X, Yang P, Zheng J, Lu C (2013) RuO_2/$TiSi_2$/graphene composite for enhanced photocatalytic hydrogen generation under visible light irradiation. Phy Chem Chem Phy 15:2793–2799
126. Yang Z, Zhang Y, Schnepp Z (2015) Soft and hard templating of graphitic carbon nitride. J Mater Chem A 27:14081–14092
127. Rhimi B, Wang C, Bahnemann D (2020) Latest progress in g-C_3N_4 based heterojunctions for hydrogen production via photocatalytic water splitting: a mini review. J Phy: Energ 2:042003
128. Hong Y, Li C, Fang Z, Luo B, Shi W (2017) Rational synthesis of ultrathin graphitic carbon nitride nanosheets for efficient photocatalytic hydrogen evolution. Carbon 121:463–471
129. Wang X, Maeda K, Thomas A, Takanabe K, Xin G, Carlsson JM, Domen K, Antonietti M (2009) A metal-free polymeric photocatalyst for hydrogen production from water under visible light. Nat Mater 8:76–80
130. Xiang Q, Yu J, Jaroniec M (2011) Preparation and enhanced visible-light photocatalytic H_2-production activity of graphene/C_3N_4 composites. J Phy Chem C 115(15):7355–7363
131. Song C, Fan M, Shi W, Wang W (2018) High-performance for hydrogen evolution and pollutant degradation of reduced graphene oxide/two-phase gC_3N_4 heterojunction photocatalysts. Environ Sci Pollut Res 25:14486–14498
132. Zou JP, Wang LC, Luo J, Nie YC, Xing QJ, Luo XB, Du HM, Luo SL, Suib SL (2016) Synthesis and efficient visible light photocatalytic H_2 evolution of a metal-free g-C_3N_4/graphene quantum dots hybrid photocatalyst. App Cat B: Environm 15(193):103–109

133. He F, Chen G, Zhou Y, Yu Y, Li L, Hao S, Liu B (2016) ZIF-8 derived carbon (C-ZIF) as a bifunctional electron acceptor and HER cocatalyst for gC_3N_4: construction of a metal-free, all carbon-based photocatalytic system for efficient hydrogen evolution. J Mater Chem A 4(10):3822–3827
134. Wang B, Zhang J, Huang F (2017) Enhanced visible light photocatalytic H_2 evolution of metal-free g-C_3N_4/SiC heterostructured photocatalysts. App Sur Sci 391:449–456
135. Yao L, Wei D, Ni Y, Yan D, Hu C (2016) Surface localization of CdZnS quantum dots onto 2D g-C_3N_4 ultrathin microribbons: highly efficient visible light-induced H_2-generation. Nano Energ 26:248–256
136. She X, Wu J, Xu H, Zhong J, Wang Y, Song Y, Nie K, Liu Y, Yang Y, Rodrigues MT, Vajtai R (2017) High efficiency photocatalytic water splitting using 2D α-Fe_2O_3/g-C_3N_4 Z-scheme catalysts. Adv Ener Mater 17:1700025
137. Martin DJ, Reardon PJT, Moniz SJ, Tang J (2014) Visible light-driven pure water splitting by a nature-inspired organic semiconductor-based system. J Am Chem Soc 36:12568–12571
138. Ong WJ, Tan LL, Ng YH, Yong ST, Chai SP (2016) Graphitic carbon nitride (g-C3N4)-based photocatalysts for artificial photosynthesis and environmental remediation: are we a step closer to achieving sustainability? Chem Rev 116:7159–7329
139. Bard AJ et al (1980) Photoelectrochemistry. Science 207:139–144
140. Xie H, Hou C, Wang H, Zhang Q, Li Y (2017) S, N co-doped graphene quantum dot/TiO_2 composites for efficient photocatalytic hydrogen generation. Nano Res Lett 1:1–8